



# Polarization effect on focal length of photonic nanojet

Yu-Jing Yang<sup>1</sup> · De-Long Zhang<sup>1</sup>

Received: 12 May 2023 / Accepted: 14 September 2023 / Published online: 4 October 2023  
© The Author(s), under exclusive licence to Springer-Verlag GmbH Germany, part of Springer Nature 2023

## Abstract

A theoretical study has been performed on effect of polarization state of incident plane wave on performance of photonic nanojet (PNJ) generated by a sphere or an ellipsoid or an elliptical cylinder scatterer, among which the sphere has a higher while the ellipsoid and elliptical cylinder have a relatively low geometric symmetry. The study shows that the polarization state of incident wave affects mainly full width at half maximum of the PNJ in case of the sphere scatterer, whilst influences mainly the focal length in case that the scatterer is an ellipsoid or elliptical cylinder. Further study focuses on the effect on the focal length of the PNJ generated by either an ellipsoid or an elliptical cylinder scatterer, and the influences of type, geometric size and orientation of scatterer on the effect. The results show that the effect prefers to take place for a scatterer with a lower symmetry, and the type, geometric size and orientation of scatterer all can influence the effect. There exists a maximum effect at a certain symmetry and the maximum effect depends on the type, geometric size and orientation of scatterer. In the case of the elliptical cylinder, the focal length of PNJ generated can increase by as much as two times as the polarization state is changed.

## 1 Introduction

Photonic nanojet (PNJ) refers to a highly focused beam generated by waves scattered by a mesoscale particle [1, 2]. It is featured by ultra-high light intensity, sub-wavelength waist and wavelength-scale propagation distance, which are characterized by light intensity enhancement, full width at half maximum (FWHM) and focal length (FL). Among these PNJ parameters, the FL is a crucial parameter that determines the application scenarios of PNJ [3]. A PNJ with a longer FL can be used to probe surface topography of sample [4], measure refractive index of medium [5], enhance Raman signal [6], and detect diameter of single particle [7, 8]. On the other hand, a PNJ with a shorter FL may find its use in high-resolution imaging of microscope [9], and power enhancement of antennas radiation [10–12]. Due to

the importance of FL, researchers have proposed a lot of methods to tailor the FL of PNJ [13–22]. The first one is to change refractive index ratio of the dielectric particle and surrounding medium on the basis of the viewpoint that a structure with a lower refractive index ratio produces a PNJ with a longer FL [13–16]. The second method is to change the shape of scatterer structure. Various structures with different shapes have been adopted to produce a PNJ with a desired FL, such as a dome [17], a hemispheric shell [18], an ellipsoid [19], a two-layer dielectric microsphere [20], a glass cuboid embedded in a dielectric cylinder [21], two-layer cylinder of high refractive-index materials [22]. Besides these traditional spherical and cylindrical structures, brothers Minin have proposed to generate a PNJ using a mesoscale particle of arbitrary three-dimensional shape [10, 11, 23], and found that a cuboid particle can generate a more symmetric beam spot than a sphere with the same size in the case of linear polarization [2]. In addition, the FL of PNJ can be also tailored by the size of scatterer. A larger scatterer is expected to produce a longer FL PNJ [24, 25].

It is worthwhile to point out that all of the preceding studies concentrate on the FL tailoring via adjusting the optical and geometrical parameters of scatterer structure. From the viewpoint of application, the change of dielectric structure is unrealistic and unfeasible for dynamical control of FL in real time and the complicated scatterer structure

✉ De-Long Zhang  
dlzhang@tju.edu.cn

<sup>1</sup> Department of Opto-electronics and Information Engineering, School of Precision Instruments and Opto-Electronics Engineering, Key Lab of Optoelectronic Information Technology (Ministry of Education), and Key Lab of Micro-Opto-Electro-Mechanical Systems (MOEMS) Technology (Ministry of Education), Tianjin University, Tianjin 300072, China

increases the difficulty in scatterer fabrication. Comparatively, it is more feasible, flexible and easier to realize the FL tailoring via controlling the polarization state of incident wave. Over the past years, a few papers have preliminarily studied polarization state effect on characteristics of PNJ [2, 26–30]. The studies concentrated on the PNJ generated by a scatterer with a higher geometric symmetry, such as a two-dimensional axis symmetric scatterer (an infinite long cylinder) [26] or a three-dimensional scatterer of spheroid or cuboid that has a circular or a square projection on the plane perpendicular to the optical axis [2, 27–30]. Higher geometric symmetry of the scatterer itself results in that the polarization state of incident wave takes significant effect on the light intensity enhancement and FWHM, while small effect on the FL of the PNJ. In addition, the previous study also focused on beam shaping and direction control of a curved PNJ by joint-adjusting the polarization state and beam size of the incident wave [31]. In overall, the effect of polarization state on the FL of PNJ was not found in all of the previous studies. Present paper demonstrates first that the FL of PNJ generated by a scatterer having a relatively low geometric symmetry can be tailored by changing the polarization state of linearly polarized incident plane wave. To achieve it, we choose either an ellipsoid or an elliptical cylinder as a scatterer and carry out a systematic investigation on effect of polarization state of incident wave on the characteristic parameter FL of the PNJs generated by them. The study focuses on the relationship between the polarization effect and the geometry of scatterer. The polarization effect is characterized by the difference of the FL of PNJs generated by a scatterer under the illumination of a plane wave with different polarization states. For comparison, the study is also carried out on a sphere scatterer.

## 2 Structural model, principle and numerical method

Figure 1 shows schematic of light scattering of an ellipsoid or elliptical cylinder. A PNJ is formed and located behind the irradiated ellipsoid or elliptical cylinder. An  $xyz$  reference frame is fixed at the center of scatterer structure for convenience. For the ellipsoid, it has a semi-major axis  $R_l$  along the  $x$  axis and two semi-minor axes  $R_s$  along both  $y$  and  $z$  axes. For the elliptical cylinder, it has a semi-major (minor) axis  $R_l$  ( $R_s$ ) along the  $x$  ( $z$ ) axis and a height  $H$  ( $= 1.4\lambda$ ) along the  $y$  axis. Here, the  $H$  parameter is chosen to ensure a positive focal length in the case that the wave is incident onto a cylinder scatterer along with its axis. Assume that the scatterer is made of  $\text{SiO}_2$  with a refractive index  $n = 1.46$  at the studied wavelength  $\lambda = 500$  nm, at which the absorption of the  $\text{SiO}_2$  is minor [32]. A plane wave polarized along  $x$ - or  $y$ -axis is incident onto

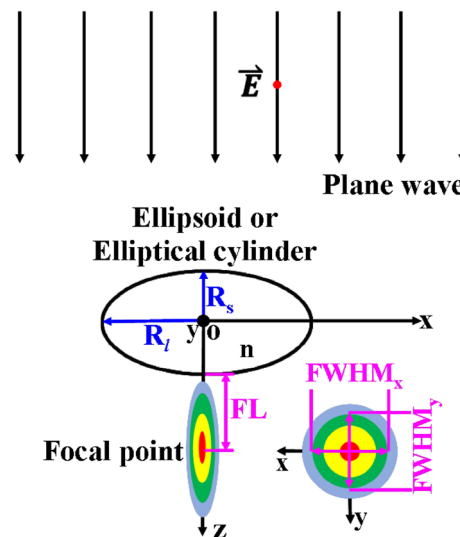


**Fig. 1** Schematic of light scattering of an ellipsoid or elliptical cylinder

the scatterer along the  $z$ -axis. It has an intensity of  $I_0$ . As shown in Fig. 1, the scattered waves interfere with each other, resulting in formation of a PNJ behind the scatterer. Figure 1 shows schematic of the PNJ projected onto  $xz$  (left) and  $xy$  (right) planes. The PNJ is usually characterized by three parameters: (1) focal length (FL), defined as the distance from the scatterer's surface to the  $z$  position where the scattered wave intensity maximizes [also called focal point as indicated in Fig. 1]; (2)  $\text{FWHM}_{x(y)}$ , defined as full width at half maximum intensity along the transversal  $x/y$ -axis at focal point; and (3) wave intensity enhancement factor, defined as the ratio of the maximum intensity  $I_{\max}$  to the incident intensity  $I_0$ .

Based on the structural model depicted in Fig. 1, we have investigated systematically the effect of wave polarization state on the performance of PNJ produced by an ellipsoid or an elliptical cylinder. For comparison, the study was also performed on a sphere scatterer. The investigation focuses on the polarization effect on the FL of PNJ. All simulations were accomplished using a commercially available program (CST Microwave Studio). A transient solver in time domain was adopted. A sufficiently fine hexahedral mesh with an inhomogeneous size ranging from  $\lambda/60$  to  $\lambda/30$  was employed to ensure an enough small iteration step. Meanwhile, a strict iterative termination condition was adopted to ensure sufficient iteration times. The strict iterative termination condition ensures the accuracy of numerical calculation, together with the sufficiently fine mesh and adaptive refinement measure. Open boundary condition, which is usually adopted to calculate the scattered field, has been adopted in our simulation.

### 3 Numerical results and discussion

#### 3.1 Polarization effect of PNJ generated by a sphere scatterer

First of all, the polarization effect is studied on a sphere structure. Figure 2a, and b shows the PNJs projected onto  $xz$  plane and generated by a sphere with  $R_1=R_s=\lambda$  under the illumination of  $x$ - or  $y$ -polarized incident wave. The white dashed line marks the focal position of PNJ. One can see that the two PNJs have the same FL. Thus, for sphere scatterer, the change of polarization state does not affect the FL of PNJ. On the other hand, the polarization state affects considerably the shape of wave spot. As shown in Fig. 2a, b, the two PNJs have considerably different widths along  $x$ -axis at the focal position. The difference is further observed for the PNJs projected onto the  $xy$  plane, as shown in Fig. 2c, and d. One can see that the PNJ generated in the case of the  $x$ -polarized incident wave has larger  $y$ -width, while the one generated in the case of the  $y$ -polarized incident wave has larger  $x$ -width. In specific, the PNJ generated in the case of the  $x$ -polarized incident wave has an  $\text{FWHM}_x$  of  $0.57\lambda$  and an  $\text{FWHM}_y$  of  $0.63\lambda$ , while that generated in the case of the  $y$ -polarized incident wave has an  $\text{FWHM}_x$  of  $0.63\lambda$  and

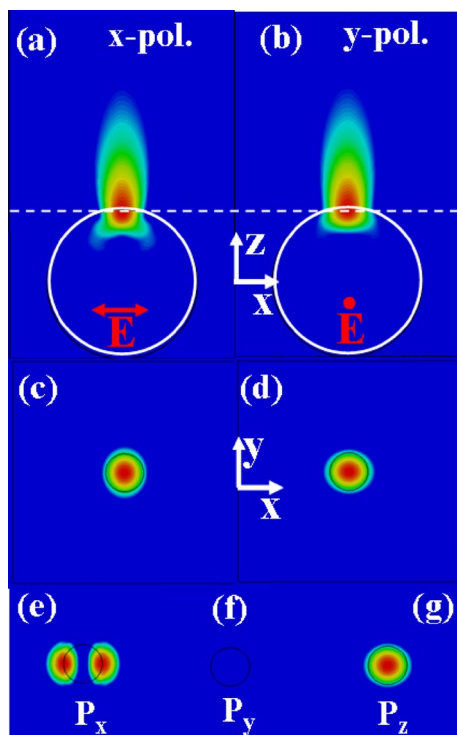


**Fig. 2** PNJ generated by a sphere with  $R_1=R_s=\lambda$  and projected onto **a, b**  $xz$  and **c, d**  $xy$  planes. **e–g** Poynting components  $P_x$ ,  $P_y$  and  $P_z$  at focal point for the PNJ generated in the case that the incident plane wave is  $y$ -polarized

an  $\text{FWHM}_y$  of  $0.57\lambda$ . In words, for a sphere scatterer, the polarization state affects mainly the FWHM while hardly the FL. Next, we try to give a qualitative explanation for the polarization effect on the FWHM on the basis of distribution feature of components of Poynting vector at the focal position. Figure 2e–g shows the distributions of  $x$ -,  $y$ -, and  $z$ -components  $P_x$ ,  $P_y$  and  $P_z$  of Poynting vector on  $xy$  plane for a PNJ generated in case that a  $y$ -polarized plane wave is incident onto a sphere scatterer. One can see that, as the incident electric field is polarized along the  $y$ -axis, the  $x$ - and  $z$ -components  $P_x$  and  $P_z$  are predominant at the focal point, and the  $x$ -component  $P_x$  reveals panda-eye-like distribution feature along  $x$ -axis and the  $z$ -component  $P_z$  shows a circular wave spot. One can anticipate that the panda-eye-like feature results in broadening of total Poynting distribution along the  $x$  axis. It is thus comprehensible that the resultant PNJ has a larger  $\text{FWHM}_x$  and a relatively small  $\text{FWHM}_y$ . As the incident plane wave is polarized along the  $x$  axis, the  $y$ -component  $P_y$  reveals panda-eye-like distribution feature along  $y$ -axis instead. As a result, the resultant PNJ has a larger  $\text{FWHM}_y$  and a relatively small  $\text{FWHM}_x$ .

#### 3.2 Polarization effect of PNJ generated by an ellipsoid or an elliptical cylinder

Next, attention is further paid to the polarization effect on the performance of PNJ generated by an ellipsoid and an elliptical cylinder.

##### 3.2.1 PNJ generated by an ellipsoid scatterer

For the ellipsoid scatterer, the study is carried out in the case that the semi-minor axis  $R_s$  is fixed at  $R_s=\lambda$  while the semi-major axis  $R_1$  varies from  $\lambda$  to  $3\lambda$ . For reference, Table 1 brings together the values of characteristic parameters of the PNJs generated in case that ellipsoids with varied  $R_1$  and fixed  $R_s=\lambda$  are irradiated by an  $x$ - or  $y$ -polarized plane wave. These parameters include the FL, wave intensity enhancement factor  $I_{\max}/I_0$ ,  $\text{FWHM}_x$  and  $\text{FWHM}_y$ . Note that the FWHM data in the case of negative FL are given in unit of  $\lambda$  in medium. One can see that, as the

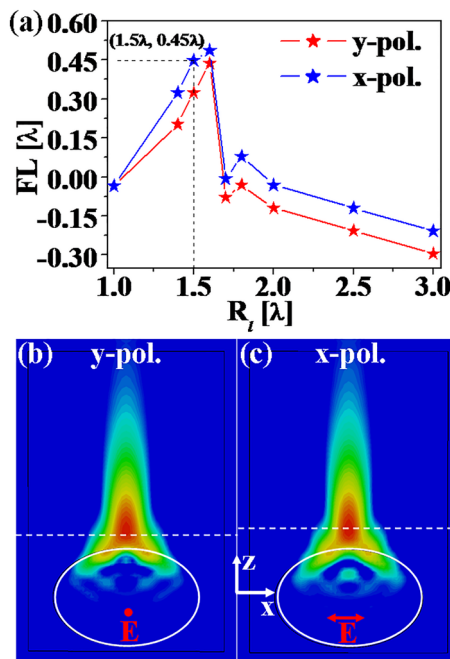
$R_1$  is increased from  $\lambda$  to  $3\lambda$ , the  $I_{\max}/I_0$  decreases from  $\sim 32$  to  $\sim 10$ , and the  $\text{FWHM}_x$  and  $\text{FWHM}_y$  change in the range of  $0.55\lambda$ – $0.80\lambda$  and  $0.48\lambda$ – $1.21\lambda$ , respectively. It is worthwhile to point out that, as  $R_1$  is larger than  $1.7\lambda$ , the PNJ generated has a negative FL and the focal spot splits into two components along  $x$ -axis. In this case, the definition for  $\text{FWHM}_x$  is no longer applicable. Next, we discuss mainly the  $R_1$  dependence of FL and polarization effect.

Figure 3a shows the  $R_1$  dependence of the FL of PNJ generated by an ellipsoid that is illuminated by a  $y$ - or  $x$ -polarized incident wave. The red and blue asterisks represent the  $y$ - and  $x$ -polarization cases, respectively. The intersection

**Table 1** FL, wave intensity enhancement factor  $I_{\max}/I_0$ ,  $\text{FWHM}_x$  and  $\text{FWHM}_y$  of PNJ generated in case that ellipsoids with varied  $R_1$  and fixed  $R_s = \lambda$  are irradiated by an  $x$ - or  $y$ -polarized plane wave

$R_1$ ( $\lambda$ )	FL ( $\lambda$ ) x-pol	FL ( $\lambda$ ) y-pol	$I_{\max}/I_0$ x-pol	$I_{\max}/I_0$ y-pol	$\text{FWHM}_x$ ( $\lambda$ ) x-pol	$\text{FWHM}_x$ ( $\lambda$ ) y-pol	$\text{FWHM}_y$ ( $\lambda$ ) x-pol	$\text{FWHM}_y$ ( $\lambda$ ) y-pol
1	-0.03	-0.03	31.87	31.89	0.57	0.63	0.63	0.57
1.4	0.32	0.20	21.05	20.15	0.55	0.69	0.55	0.48
1.5	0.45	0.32	20.34	20.48	0.60	0.74	0.56	0.53
1.6	0.49	0.44	15.87	15.44	0.73	0.80	0.61	0.61
1.7	-0.01	-0.08	15.01	15.42	-	-	0.89	0.82
1.8	0.08	-0.03	13.35	14.24	-	-	0.47	0.57
2	-0.03	-0.12	13.46	13.91	-	-	0.82	0.67
2.5	-0.12	-0.21	10.60	11.54	-	-	0.95	0.64
3	-0.21	-0.30	9.68	9.53	-	-	1.21	0.63

Note that in the case of negative FL the FWHM data are given in unit of  $\lambda$  in medium



**Fig. 3** **a**  $R_1$  dependence of FL of PNJ generated by an ellipsoid with  $R_s = \lambda$ . **b**, **c** PNJs projected onto the  $xz$  plane and generated by the ellipsoid with  $R_1 = 1.5\lambda$  and  $R_s = \lambda$  in the case of an irradiation by a  $y$ - or  $x$ -polarized incident wave

of two plots takes place at  $R_1 = R_s = \lambda$ , which corresponds to a spherical scatterer. It means that the two PNJs generated by a sphere that is irradiated by a  $y$ - or  $x$ -polarized incident wave have the equal FL. This is consistent with the preceding result of the sphere scatterer. In words, the PNJ generated by a sphere scatterer has less polarization effect on the FL. Back to Fig. 3a. As  $R_1$  is larger than  $\lambda$ , the FL of the PNJ generated by the  $x$ -polarized incident wave has a value definitely larger than that by the  $y$ -polarized incident wave, indicating that the FL shows definite polarization effect. The effect changes slightly from one  $R_1$  value to another and maximizes as  $R_1 = 1.5\lambda$ . Aiming at the largest polarization

effect, which takes place at  $R_1 = 1.5\lambda$ , we have calculated the PNJs projected onto  $xz$  plane in the case of an irradiation by a  $y$ - or  $x$ -polarized incident wave. The results are shown in Fig. 3b, c. The white dashed lines mark the focal positions of two PNJs, and the red full dot and arrow symbols represent the polarization directions along  $y$  and  $x$ -axes, respectively. One can see that the FLs of the two PNJs show clear polarization effect.

The polarization effect is related to the geometry of scatterer structure. As we know, a scatterer structure having a larger size tends to generate a PNJ with a larger FL [13]. The focal position of the PNJ is correlated with the focusing of wave in the meridional and sagittal planes. Consider that an ellipsoid has a semi-minor axis  $R_s$  (along the  $y$ -axis) smaller than its semi-major axis  $R_1$  (along the  $x$ -axis). This means that the scatterer has a smaller size along the  $y$ -axis and a stronger confinement to scattered wave along this axis. As a result, the PNJ has a smaller FL along the  $y$  direction. As a plane wave polarized along the  $y$ -axis is incident onto this ellipsoid scatterer, the electric field oscillates along the  $y$ -axis and mainly interacts with the structure along  $y$ -axis. As a result, the interaction of electric field and the structure along the  $y$ -axis plays a dominant role in the formation of PNJ, and thereby a PNJ with a smaller FL can be obtained. On the other hand, the scatterer structure has a larger size along the  $x$ -axis and hence a weaker confinement to waves in this direction. As a plane wave polarized along the  $x$ -axis is incident onto the structure, the electric field oscillates along the  $x$ -axis and mainly interacts with the structure along the  $x$ -axis. Consequently, the interaction of electric field and the structure along the  $x$ -axis plays a dominant role in the formation of PNJ, and a PNJ with a larger FL can be thus obtained. Furthermore, for a wave polarized along an arbitrary direction in  $xy$  plane and incident onto a scatterer structure, its electric field can be decomposed into  $x$ - and  $y$ -components. In this case, the formation of PNJ is determined by the interactions between the scatterer structure and these two electric field components. In addition, the incident wave with a

larger  $x$ -component tends to obtain a PNJ with larger FL, while that with a larger  $y$ -component is expected to obtain a PNJ with smaller FL. Maximal and minimal FLs are obtained as the incident wave is purely  $x$ - and  $y$ -polarized, respectively, and the FL with a median value is obtained for the incident wave polarized along an arbitrary direction in  $xy$  plane. As the polarization state is changed, the proportions of  $x$ - and  $y$ -components of electric field change correspondingly, resulting in the change of FL. The change of geometrical parameters renders the confinement to waves in different directions changed, and hence makes the FL changed. This point was verified by the variational relationship between  $R_1$  and the FL, as shown in Fig. 3a.

In addition, we note from Table 1 and Fig. 3a that the polarization effect on the FL shows a non-monotonic dependence on  $R_1$ . The observation may be explained as follows. As pointed out above, the FL of PNJ has a negative value and the focal spot splits into two components in case that  $R_1 > 1.6\lambda$ . The two features result in a sudden change of the PNJ properties and hence the non-monotonic

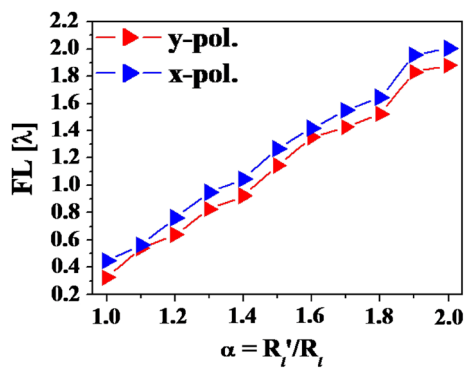


Fig. 4  $\alpha$  ( $=R_1'/R_1$ ) dependence of FL of PNJ generated by the ellipsoid illuminated by a  $y$ -polarized (red) or  $x$ -polarized (blue) plane wave

dependence of polarization effect of FL on  $R_1$ . In this case, the PNJ is no longer the normal PNJ with just one focused spot. Similar non-monotonic feature is also observed in the case that an elliptical cylinder scatterer is considered below, and the relevant description is no longer presented in the following context for saving space.

As pointed out above, the maximum polarization effect of the FL happens in the case that the ellipsoid has  $R_1 = 1.5\lambda$  and  $R_s = \lambda$ . We have selected  $R_1 = 1.5\lambda$  and  $R_s = \lambda$  as the fundamental geometrical parameters and further investigated the polarization effect as a function of the overall varying factor of the size of ellipsoid scatterer, named  $\alpha = R_1'/R_1 = R_s'/R_s$ , where  $R_1$  and  $R_s$  were fixed at  $1.5\lambda$  and  $\lambda$ , respectively, and  $R_1'$  and  $R_s'$  represent the sizes that the ellipsoid scatterer is magnified or reduced by  $\alpha$ -fold. Figure 4 shows the FL of PNJ calculated as a function of the  $\alpha$  in the range of 1.0–2.0. The red/blue plot represents the illumination by a  $y$ -/ $x$ -polarized incident wave. We can see that, as the overall varying factor  $\alpha$  is increased from 1.0 to 2.0, the FL value increases significantly. This is the case whether the PNJ is generated by the  $x$ - or  $y$ -polarized incident wave. We also note that the PNJ generated by the  $x$ -polarized incident wave has a larger FL value, and the polarization effect of FL changes little with the  $\alpha$  value, suggesting that an overall change of the size of scatterer affects little the polarization effect of the FL. This is comprehensive because the overall change of the size of scatterer does not change the geometric shape feature of the ellipsoid scatterer, and hence does not affect the polarization effect noticeably. For reference, Table 2 brings together the values of characteristic parameters of the PNJs generated in case that ellipsoids with varied overall varying factor  $\alpha$  under the illumination by a  $y$ - or  $x$ -polarized wave.

Besides the symmetry and overall varying factor considered above, the orientation of the ellipsoid may also influence the polarization effect. We have studied the influence by rotating the ellipsoid ( $R_1 = 1.5\lambda$  and  $R_s = \lambda$ ) either around

Table 2 FL,  $I_{\max}/I_0$ , FWHM<sub>x</sub> and FWHM<sub>y</sub> of PNJs generated by ellipsoids with varied overall varying factor  $\alpha$  under the illumination of  $y$ - or  $x$ -polarized plane wave

$\alpha$	FL ( $\lambda$ ) x-pol	FL ( $\lambda$ ) y-pol	$I_{\max}/I_0$ x-pol	$I_{\max}/I_0$ y-pol	FWHM <sub>x</sub> ( $\lambda$ ) x-pol	FWHM <sub>x</sub> ( $\lambda$ ) y-pol	FWHM <sub>y</sub> ( $\lambda$ ) x-pol	FWHM <sub>y</sub> ( $\lambda$ ) y-pol
1	0.45	0.32	21.63	20.48	0.60	0.74	0.56	0.53
1.1	0.56	0.54	22.92	22.10	0.62	0.73	0.56	0.53
1.2	0.76	0.64	25.30	25.08	0.59	0.78	0.61	0.54
1.3	0.95	0.83	27.50	26.41	0.61	0.81	0.62	0.57
1.4	1.05	0.92	27.20	26.96	0.66	0.89	0.62	0.56
1.5	1.27	1.14	27.73	27.17	0.66	0.85	0.69	0.63
1.6	1.42	1.35	27.88	28.17	0.70	0.89	0.70	0.61
1.7	1.55	1.43	29.11	29.78	0.71	0.91	0.73	0.63
1.8	1.65	1.52	31.39	28.55	0.79	1.18	0.66	0.66
1.9	1.96	1.83	30.73	28.37	0.73	1.06	0.78	0.79
2	2.00	1.88	30.19	29.84	0.77	1.08	0.81	0.79

The other parameters are  $R_1 = 1.5\lambda$  and  $R_s = \lambda$

the  $z$ -axis with an angle  $\theta$  or around the  $y$ -axis with an angle  $\phi$  all in the range of  $0^\circ$ – $90^\circ$ . Figure 5a shows rotation angle  $\theta$  dependence of parameters of FL,  $I_{\max}/I_0$ ,  $\text{FWHM}_x$  and  $\text{FWHM}_y$  of PNJs. The red/blue plots represent the cases of  $y$ -/ $x$ -polarized wave illumination, respectively. The two cases  $\theta=0^\circ$  and  $90^\circ$  correspond to Figs. 3b, c and 5b, c, respectively. Figure 6a shows rotation angle  $\phi$  dependences. The two cases  $\phi=0^\circ$  and  $90^\circ$  correspond to Figs. 3b, c and 6b, c, respectively.

1. Attention is first paid to the effect of  $\theta$  or  $\phi$  on the FL. As shown in Figs. 5a and 6a, all of the FL plots show a monotonous dependence on the rotation angle  $\theta$  or  $\phi$ , and the  $\phi$  dependence is stronger than the  $\theta$  dependence. As the  $\theta$  ( $\phi$ ) is increased from  $0^\circ$  to  $90^\circ$ , the FL changes by  $\sim 0.15\lambda$  ( $\sim 0.6\lambda$ ). As the  $\theta$  ( $\phi$ ) changes, the polarization effect has a maximum  $\sim 0.15\lambda$  ( $\sim 0.21\lambda$ ). In addition,

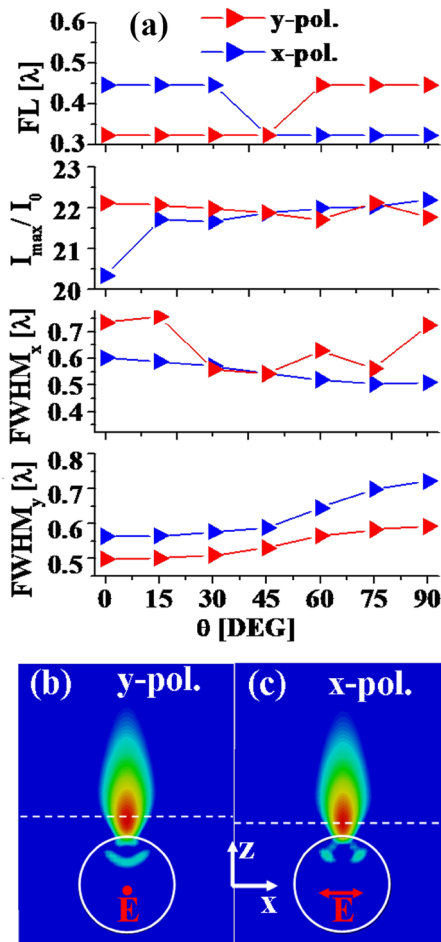


**Fig. 5** a Rotation angle  $\theta$  dependence of FL,  $I_{\max}/I_0$ ,  $\text{FWHM}_x$  and  $\text{FWHM}_y$  of PNJ generated by rotating the ellipsoid around  $z$ -axis and illuminating with a plane wave polarized along  $y$ - (red) or  $x$ -axis (blue). b, c PNJs projected onto the  $xz$  plane and generated in the case of  $\theta=90^\circ$

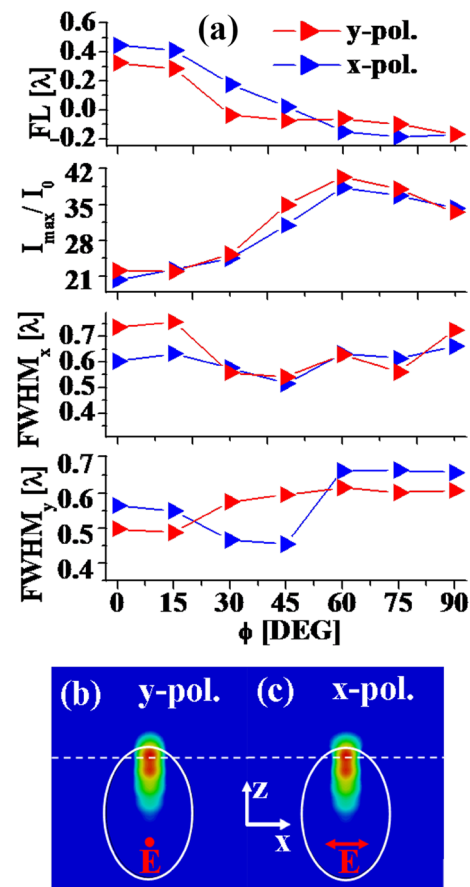


**Fig. 6** a Rotation angle  $\phi$  dependence of FL,  $I_{\max}/I_0$ ,  $\text{FWHM}_x$  and  $\text{FWHM}_y$  of PNJ generated by rotating the ellipsoid around  $y$ -axis and illuminating with a plane wave polarized along  $y$ - (red) or  $x$ -axis (blue). Note that in the case of negative FL the FWHM data are given in unit of  $\lambda$  in medium. b, c PNJs projected onto the  $xz$  plane and generated in the case of  $\phi=90^\circ$ , respectively. At  $\theta=90^\circ$ , however, the major and minor axes of the ellipsoid orient along the  $y$  and  $x$  axes, respectively. The two cases are equivalent to the exchange of major and minor axes of the ellipsoid, resulting in that the polarization effects on the FL at  $\theta=90^\circ$  and  $0^\circ$  are equal in value and opposite in sign. Figure 5b, c shows the PNJs projected onto the  $xz$  plane and generated in the case of  $\theta=90^\circ$ . One can see that the polarization effect is discernible

the polarization effect shows a sign change at  $\theta$  around  $45^\circ$ . As  $\theta < 45^\circ$ , the FL in the case of  $x$ -polarized wave illumination is larger than that in the case of  $y$ -polarized wave illumination. As  $\theta > 45^\circ$ , a reversed feature is observed. The FL in the case of  $y$ -polarized wave illumination is larger. At  $\theta \approx 45^\circ$ , the FLs of two PNJs generated in the two cases of  $x$ - and  $y$ -polarizations have the equal values of  $0.32\lambda$ . This is because, as  $\theta=45^\circ$ , the rotated ellipsoid orients along the diagonal direction of  $xy$  plane and the electric fields of  $x$ - and  $y$ -polarized waves have the same components in that direction, and thereby the polarization has little effect on the FL. Similar feature of sign change of polarization effect on FL

is also observed for  $\phi \approx 50^\circ$  as shown in Fig. 6a. The polarization effect on the FL at  $\theta = 90^\circ$  has the same value but opposite signs as that at  $\theta = 0^\circ$ . At  $\theta = 0^\circ$ , the major and minor axes of the ellipsoid orient along the  $x$  and  $y$  axes.

We also note that the polarization effect minimizes at  $\phi = 90^\circ$ , i. e., the FLs in the two cases of  $x$ - and  $y$ -polarizations have the same value. This can be explained from the viewpoint of  $\phi$ -rotation-induced change of geometry of the ellipsoid projected onto the  $xy$  plane. As the ellipsoid rotates around  $y$ -axis from  $0^\circ$  to  $90^\circ$ , the projection of ellipsoid onto the  $xy$  plane changes gradually from an ellipse to a circle, resulting in cancellation of the polarization effect on FL. Figure 6b, c shows the PNJs projected onto the  $xz$  plane and generated in the case of  $\phi = 90^\circ$ . One can see that the polarization effect is indiscernible.

- We can see from Figs. 5a and 6a that the  $I_{\max}/I_0$  of PNJ changes little with  $\theta$  but considerably with  $\phi$ . The different features are associated with rotation-induced change of geometric area of the ellipsoid projected onto the  $xy$  plane. As we know, the  $I_{\max}/I_0$  of PNJ is closely related to geometric area of a scatterer projected onto the plane perpendicular to the optical axis. In the case of  $\theta$ -rotation, the geometric area of the ellipsoid projected onto the  $xy$  plane keeps constant. In the case of  $\phi$ -rotation, however, it reduces as the  $\phi$  is increased. It is thus comprehensive that the  $I_{\max}/I_0$  of PNJ changes largely with  $\phi$  while little with  $\theta$ . We also note from Figs. 5a and 6a that the influence of the rotation on the polarization effect of  $I_{\max}/I_0$  is small in both cases of  $\theta$  and  $\phi$ .
- As shown in Figs. 5a and 6a, the  $\text{FWHM}_y$  of PNJ changes weakly with both  $\theta$  and  $\phi$ . This is also the case for the  $\text{FWHM}_x$  in the case of  $x$ -polarization. In the case of  $y$ -polarization, however, the  $\text{FWHM}_x$  changes more remarkably with  $\theta$  or  $\phi$ , resulting in that the influence of the rotation on the polarization effect of the  $\text{FWHM}_x$  is more obvious than that of the  $\text{FWHM}_y$ .

In words, the orientation of ellipsoid is also a key factor in tailoring the performance of PNJ. It also influences definitely the polarization effect on both FL and  $\text{FWHM}_x$ . These orientation effects are associated with rotation-induced geometric change of the ellipsoid scatterer projected onto the  $xy$  plane and  $z$  axis [e. g. the  $\phi$ -rotation induces the size change of the ellipsoid projected onto the  $z$  axis and hence the change of FL, as observed in Fig. 6a].

### 3.2.2 PNJ generated by an elliptical cylinder scatterer

The polarization effect on the FL is further studied on an elliptical cylinder. Two cases that the polarized plane wave is

incident along the direction either perpendicular or parallel to the cylinder axis ( $z$ -axis) have been considered. Figure 7a shows the  $R_1$  dependence of FL of the PNJ generated by an elliptical cylinder with  $R_s = \lambda$  and a height  $H = 1.4\lambda$  in case that the  $y$ - or  $x$ -polarized plane wave is incident along the direction perpendicular to the cylinder axis. The red and blue asterisks represent the FLs of PNJs generated in the cases of the irradiation by  $y$ - and  $x$ -polarized waves, respectively. One can see that two FL plots show similar non-monotonous feature. The polarization effect of the FL is quite small. As the  $R_1$  changes from  $1.5\lambda$  to  $2.5\lambda$ , the polarization effect of the FL changes slightly within  $0.05\lambda$ – $0.17\lambda$  and maximizes at  $R_1 = 2\lambda$ . For convenience, Table 3 brings together the values of characteristic parameters of the PNJs.

Aiming at the largest polarization effect, which takes place at  $R_1 = 2\lambda$ , we have calculated the PNJs projected onto  $xz$  plane in the case of an irradiation by a  $y$ - or  $x$ -polarized incident wave. The results are shown in Fig. 7b, c. The white dashed lines mark the focal positions of two PNJs, and the red full dot and arrow symbols represent the polarization directions along  $y$ - and  $x$ -axes, respectively. One can see that the FL difference of two PNJs is affirmative.

In the case that the cylinder axis is perpendicular to the  $z$ -axis, the cross section of the scatterer projected onto the  $xy$  plane is a rectangle in fact. In the case that the cylinder axis is parallel to the  $z$ -axis, however, the projection onto the  $xy$  plane is an ellipse. The two projections have different geometric shape features: the ellipse has a continuously varying edge, while the rectangle has a straight

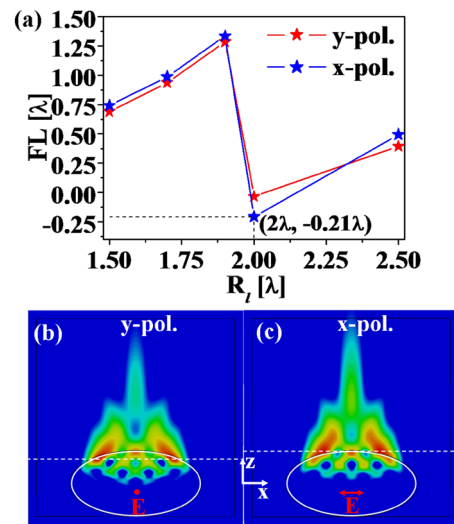


**Fig. 7** a  $R_1$  dependence of FL of PNJ generated by an elliptical cylinder with  $R_s = \lambda$  and  $H = 1.4\lambda$  in case that the  $y$ - or  $x$ -polarized plane wave is incident along the direction perpendicular to the cylinder axis. b, c PNJs projected onto the  $xz$  plane and generated by an elliptical cylinder with  $R_1 = 2\lambda$ ,  $R_s = \lambda$  and  $H = 1.4\lambda$  in the case of an illumination by a  $y$ - or  $x$ -polarized plane wave

**Table 3** FL,  $I_{\max}/I_0$ , FWHM<sub>x</sub> and FWHM<sub>y</sub> of PNJ generated by an elliptic cylinder with varied  $R_1$  and fixed  $R_s = \lambda$  and  $H = 1.4\lambda$  in case that the  $y$ - or  $x$ -polarized plane wave is incident along the direction perpendicular to the cylinder axis

$R_1 (\lambda)$	FL ( $\lambda$ ) x-pol	FL ( $\lambda$ ) y-pol	$I_{\max}/I_0$ x-pol	$I_{\max}/I_0$ y-pol	FWHM <sub>x</sub> ( $\lambda$ ) x-pol	FWHM <sub>x</sub> ( $\lambda$ ) y-pol	FWHM <sub>y</sub> ( $\lambda$ ) x-pol	FWHM <sub>y</sub> ( $\lambda$ ) y-pol
1.5	0.74	0.69	23.38	21.67	0.58	0.63	0.66	0.62
1.7	0.99	0.94	20.04	17.18	0.64	0.75	0.75	0.71
1.9	1.33	1.28	16.55	14.76	0.7	0.81	0.88	0.88
2	-0.03	-0.21	12.48	14.45	-	-	0.66	0.58
2.5	0.49	0.4	11.51	11.87	-	-	0.53	0.5

Note that in the case of negative FL the FWHM data are given in unit of  $\lambda$  in medium

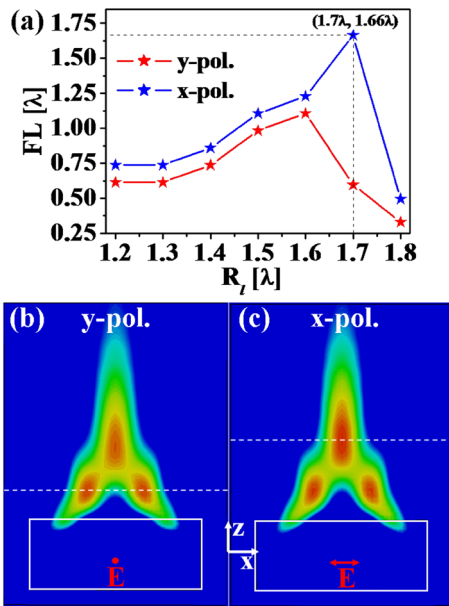


**Fig. 8** **a**  $R_1$  dependence of FL of PNJ generated by an elliptic cylinder with  $R_s = \lambda$  and  $H = 1.4\lambda$  in case that a  $y$ - or  $x$ -polarized plane wave is incident along the cylinder axis ( $z$ -axis). **b**, **c** PNJs projected onto the  $xz$  plane and generated by the elliptic cylinder with  $R_1 = 1.7\lambda$ ,  $R_s = \lambda$  and  $H = 1.4\lambda$  in the case that a  $y$ - or  $x$ -polarized plane wave is incident along the cylinder axis ( $z$ -axis)

edge, suggesting that two cases may have different polarization effects of the FL. To make the argument clear, an independent study was carried out on polarization effect of the FL in the case that a  $y$ - or  $x$ -polarized plane wave is incident along the cylinder axis ( $z$ -axis) and  $R_s = \lambda$  and  $H = 1.4\lambda$ . Figure 8a shows the FL calculated as a function of  $R_1$ . We note that a PNJ with a larger FL is generated as the elliptic cylinder has a  $R_1$  larger than  $R_s (= \lambda)$  and it is irradiated by an  $x$ -polarized incident wave, i. e., for a given  $R_1$  value, the FL in the case of  $x$ -polarization is larger than that in the case of  $y$ -polarization. The feature is consistent with the case of ellipsoid scatterer as demonstrated above. We also note from Fig. 8a that two FL plots also show similar non-monotonous feature and peak at  $R_1 = 1.7\lambda$  in the case of  $x$ -polarization and  $R_1 = 1.6\lambda$  in the case of  $y$ -polarization. It appears that the FL of PNJ

generated in the case that the cylinder axis is parallel to the  $z$ -axis shows more obvious polarization effect than that generated in the case that the cylinder axis is perpendicular to the  $z$ -axis. As the  $R_1$  changes from  $1.2\lambda$  to  $1.8\lambda$ , the polarization effect of FL changes within  $0.23\lambda - \lambda$ , which far exceeds the varying range in the case that the cylinder axis is perpendicular to the  $z$ -axis,  $0.05\lambda - 0.17\lambda$ , as given above. Aiming at the maximal polarization effect, which happens as  $R_1 = 1.7\lambda$ , we have calculated the PNJs projected onto  $xz$  plane in the case of an irradiation by a  $y$ - or  $x$ -polarized incident wave. The results are shown in Fig. 8b and c. The focal points are marked with the white dashed lines. We can see that the polarization effect on the FL is quite evident. For convenience, Table 4 brings together the values of characteristic parameters of the PNJs generated in case that a  $y$ - or  $x$ -polarized plane wave is incident along the cylinder axis ( $z$ -axis).

We have further studied the wave intensity distribution features of the PNJ generated by the elliptic cylinder in case that the maximal polarization effect takes place. Figure 9a–c shows the wave intensity distribution along the  $z$ -axis and transverse  $y$ - and  $x$ -axes of the PNJ generated by the elliptical cylinder with  $R_1 = 1.7\lambda$ ,  $R_s = \lambda$  and  $H = 1.4\lambda$  in case that a  $y$ - (red curve) or  $x$ -polarized (blue plot) plane wave is incident along the cylinder axis ( $z$ -axis). The black dashed lines in Fig. 9a indicate the focal positions. The curves in Fig. 9b, c are taken from the focal positions.

One can see from Fig. 9a that the PNJ generated in the case of  $x$ -polarized incident plane wave has a larger FL than that generated in the case of  $y$ -polarized incident plane wave, and the polarization effect of the FL is larger than  $\lambda$ . In Fig. 9b, the blue distribution curve, which corresponds to the  $x$ -polarized incident wave, is broader than the red curve concerning with the  $y$ -polarization. This is consistent with the sphere scatterer case, in which, as demonstrated above, a PNJ having a larger FWHM along the  $y$ -axis is generated as a spherical scatterer is illuminated with an  $x$ -polarized incident wave. The preceding observation shows that the polarization state also affects the FWHM of PNJ generated by an elliptical cylinder scatterer. In Fig. 9c, the wave intensity distribution features of the red/blue curve match with the wave spots marked with the dashed white lines in Fig. 8b, c.



**Table 4** FL,  $I_{\max}/I_0$ ,  $\text{FWHM}_x$  and  $\text{FWHM}_y$  of PNJ generated by an elliptic cylinder with varied  $R_1$  and fixed  $R_s = \lambda$  and  $H = 1.4\lambda$  in case that a y- or x-polarized plane wave is incident along the cylinder axis (z-axis)

$R_1 (\lambda)$	FL ( $\lambda$ ) x-pol	FL ( $\lambda$ ) y-pol	$I_{\max}/I_0$ x-pol	$I_{\max}/I_0$ y-pol	$\text{FWHM}_x (\lambda)$ x-pol	$\text{FWHM}_x (\lambda)$ y-pol	$\text{FWHM}_y (\lambda)$ x-pol	$\text{FWHM}_y (\lambda)$ y-pol
1.2	0.74	0.61	19.35	19.15	0.64	0.69	0.61	0.55
1.3	0.86	0.74	17.9	17.9	0.69	0.79	0.59	0.52
1.4	1.11	0.98	16.12	16.15	0.79	0.96	0.62	0.55
1.5	1.23	1.11	14.33	14.15	0.87	1.1	0.68	0.62
1.6	1.67	0.53	12.48	12.31	1.09	1.4	0.71	0.65
1.7	0.5	0.33	11.06	11	1.11	0.93	0.81	0.45
1.8	0.74	0.74	11.19	10.55	0.89	1.12	–	0.5

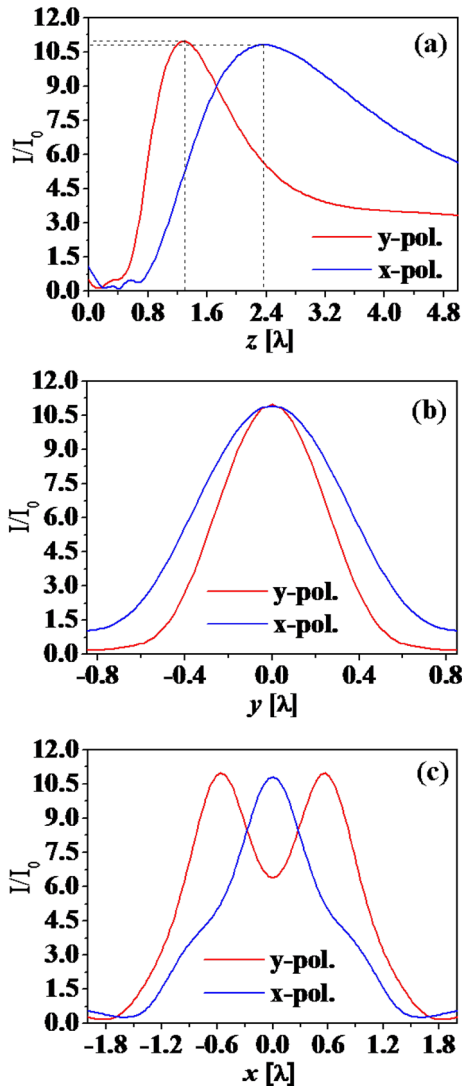


**Fig. 9** Wave intensity distribution along **a** z-, **b** y- and **c** x-axis of the PNJ generated by the elliptical cylinder with  $R_1 = 1.7\lambda$ ,  $R_s = \lambda$  and  $H = 1.4\lambda$  in case that a y- or x-polarized plane wave is incident along the cylinder axis (z-axis)

### 4 Conclusion

We have investigated the effect of polarization state of incident wave on characteristic parameters of a PNJ generated by a sphere or an ellipsoid or an elliptical cylinder scatterer. Study shows that, in addition to the geometry of scatterer, polarization state of incident wave is another key factor in tailoring the performance of PNJ generated by a scatterer. For a PNJ generated by a sphere, which has a higher geometric symmetry, the polarization state of incident wave affects mainly its  $\text{FWHM}_{x(y)}$  while hardly its FL. For an ellipsoid or elliptical cylinder scatterer, which has a relatively low symmetry, the polarization state affects mainly the focal length as a result of interaction between the polarized electric field and the scatterer. Further study shows that the polarization state effect on the FL occurs for a lower-symmetry scatterer. It is influenced by type, geometric size and orientation of scatterer. There exists a maximum effect at a certain symmetry, and the maximum effect depends on the type, geometric size and orientation of scatterer. In particular, for a PNJ generated by an elliptical cylinder, as the wave is incident along the cylinder axis, the change of polarization state may cause FL alteration by as much as two times. On the other hand, an overall size increase or decrease of the scatterer affects little the polarization effect on the FL.

In words, polarization state of incident wave is a more feasible, effective, and convenient factor in tailoring the FL of a PNJ generated by a scatterer than the others, such as the geometry of scatterer. With a properly designed polarization state, a PNJ with a desired focal length would be obtained for various application purposes.

**Acknowledgements** This work is supported by the National Natural Science Foundation of China under Project no. 61875148, and by Key Awards Program of Cultivating Outstanding Innovative Postgraduates in Arts and Sciences of Tianjin University, under Project no. C1-2022-002.

**Author contributions** "Y.J.Y.wrote the main manuscript text and D.L.Z. reviewed the manuscript.

## Declarations

**Competing interests** The authors declare no competing interests.

## References

- Z.G. Chen, A. Taflove, V. Backman, Photonic nanojet enhancement of backscattering of light by nanoparticles: a potential novel visible-light ultramicroscopy technique. *Opt. Express* **12**(7), 1214–1220 (2004)
- I.V. Minin, O.V. Minin, *Diffractive Optics and Nanophotonics-Resolution Below the Diffraction Limit* (Springer, Cham, 2016)
- J.L. Zhu, L.L. Goddard, All-dielectric concentration of electromagnetic fields at the nanoscale: the role of photonic nanojets. *Nanoscale Adv.* **1**, 4615 (2019)
- M. Duocastella, F. Tantussi, A. Haddadpour, R.P. Zaccaria, A. Jacassi, G. Veronis, A. Diaspro, F.D. Angelis, Combination of scanning probe technology with photonic nanojets. *Sci. Rep.* **7**(1), 3474 (2017)
- Y.C. Li, X.S. Liu, X.H. Xu, H.B. Xin, Y. Zhang, B.J. Li, Red-blood-cell waveguide as a living biosensor and micromotor. *Adv. Funct. Mater.* **29**(50), 1905568 (2019)
- H.S. Patel, P.K. Kushwaha, M.K. Swami, Photonic nanojet assisted enhancement of raman signal: effect of refractive index contrast. *J. Appl. Phys.* **123**(2), 023102 (2018)
- H. Yang, M. Cornaglia, M.A. Gijs, Photonic nanojet array for fast detection of single nanoparticles in a flow. *Nano Lett.* **15**(3), 1730–1735 (2015)
- G.Q. Gu, J. Song, M. Chen, X. Peng, H.D. Liang, J.L. Qu, Single nanoparticle detection using a photonic nanojet. *Nanoscale* **10**(29), 14182–14189 (2018)
- Y.J. Yang, D.L. Zhang, P.R. Hua, High-resolution perfect imaging of micro/nanojet. *Results Phys.* **38**, 105616 (2022)
- V. Pacheco-Pena, M. Beruete, I.V. Minin, O.V. Minin, Terajets produced by dielectric cuboids. *Appl. Phys. Lett.* **105**(8), 3966 (2014)
- V. Pacheco-Pena, M. Beruete, I.V. Minin, O.V. Minin, Multifrequency focusing and wide angular scanning of terajets. *Opt. Lett.* **40**(2), 245–248 (2015)
- Karabchevsky, A.: Development of mesoscale photonics and plasmonics: a tribute to the jubilee of Professors I. V. Minin, O.V. Minin. In: *Photon and Plasmonics at the Mesoscale* (SPIE), vol. 11368, pp. 44–53 (2020)
- Y.J. Yang, D.L. Zhang, P.R. Hua, Ultra-narrow and ultra-strong nanojet for nanopatterning and nanolithography. *Optik* **255**, 168726 (2022)
- P. Wu, J. Li, K. Wei, W. Yue, Tunable and ultra-elongated photonic nanojet generated by a liquid-immersed core-shell dielectric microsphere. *Appl. Phys. Exp.* **8**(11), 112001 (2015)
- A. Darafsheh, Influence of the background medium on imaging performance of microsphere-assisted super-resolution microscopy. *Opt. Lett.* **42**(4), 735–738 (2017)
- G.Q. Gu, R. Zhou, Z.C. Chen, H.Y. Xu, G.X. Cai, Z.P. Cai, M.H. Hong, Super-long photonic nanojet generated from liquid-filled hollow microcylinder. *Opt. Lett.* **40**(4), 625–628 (2015)
- C.B. Lin, Y.T. Lee, C.Y. Liu, Optimal photonic nanojet beam shaping by mesoscale dielectric dome lens. *J. Appl. Phys.* **127**(24), 243110 (2020)
- H.Y. Zhu, Z.C. Chen, T.C. Chong, M.H. Hong, Photonic jet with ultralong working distance by hemispheric shell. *Opt. Express* **23**(5), 6626–6633 (2015)
- K. Shalin, N. Andrey, K. Alina, S.S. Alexander, A photonic nanojet as tunable and polarization-sensitive optical tweezers. *Ann. Phys.* **530**(9), 1800129 (2018)
- Y.C. Shen, L.H.V. Wang, J.T. Shen, Ultralong photonic nanojet formed by a two-layer dielectric microsphere. *Opt. Lett.* **39**(14), 4120–4123 (2014)
- J.M. Yang, P. Twardowski, P. Gerard, Y. Duo, J. Fontaine, S. Lecler, Ultra-narrow photonic nanojets through a glass cuboid embedded in a dielectric cylinder. *Opt. Express* **26**(4), 3723–3731 (2018)
- Z. Zhen, Y. Huang, Y. Feng, Y. Shen, Z. Li, An ultranarrow photonic nanojet formed by an engineered two-layer microcylinder of high refractive-index materials. *Opt. Express* **27**(6), 9178–9188 (2019)
- I.V. Minin, O.V. Minin, Y.E. Geints, Localized EM and photonic jets from non-spherical and non-symmetrical dielectric mesoscale objects: brief review. *Ann. Phys.-Berlin* **527**(7–8), 491–497 (2015)
- G.S. He, H.Y. Qin, Q.D. Zheng, Rayleigh, Mie, and Tyndall scatterings of polystyrene microspheres in water: wavelength, size, and angle dependences. *J. Appl. Phys.* **105**(2), 023110 (2009)
- B.S. Lukiyanchuk, R. Paniagua-Domínguez, I.V. Minin, O.V. Minin, Z. Wang, Refractive index less than two: photonic nanojets yesterday, today and tomorrow. *Opt. Mater. Express* **7**(6), 1820–1847 (2017)
- S. Zhou, Effects of light polarization in photonic nanojet. *Quant. Electron* **51**(112), 1–8 (2019)
- Y. Liu, B. Wang, Z. Ding, Influence of incident light polarization on photonic nanojet. *Chin. Opt. Lett.* **9**(7), 072901 (2011)
- R. Chen, J. Lin, P. Jin, M. Cada, Y. Ma, Photonic nanojet beam shaping by illumination polarization engineering. *Opt. Commun.* **456**, 124593 (2020)
- F.P. Wu, J.J. Wang, Z.C. Cui, S. Aihoon, P. Briard, Y.P. Han, Polarization-sensitive photonic jet of a dielectric sphere excited by a zero-order Bessel beam. *J. Quant. Spectrosc. Ra.* **280**, 108093 (2022)
- Y. Jia, R. Li, W. Zhuang, J. Liang, Photonic nanojet generated by a spheroidal particle illuminated by a vector Bessel beam. *Results Opt.* **4**, 100106 (2021)
- C.Y. Liu, H.J. Chung, O.V. Minin, I.V. Minin, Shaping photonic hook via well-controlled illumination of finite-size graded-index micro-ellipsoid. *J. Opt.* **22**(8), 085002 (2020)
- I.H. Malitson, Interspecimen comparison of the refractive index of fused silica. *J. Opt. Soc. Am.* **55**(10), 1205–1208 (1965)

**Publisher's Note** Springer Nature remains neutral with regard to jurisdictional claims in published maps and institutional affiliations.

Springer Nature or its licensor (e.g. a society or other partner) holds exclusive rights to this article under a publishing agreement with the author(s) or other rightsholder(s); author self-archiving of the accepted manuscript version of this article is solely governed by the terms of such publishing agreement and applicable law.